Influence of PWM on the Proximity Loss in Permanent-Magnet Brushless AC Machines

S. Iwasaki, Rajesh P. Deodhar, *Senior Member, IEEE*, Yong Liu, Adam Pride, *Member, IEEE*, Z. Q. Zhu, *Fellow, IEEE*, and Jonathan James Bremner

***Abstract*—A winding copper loss can be significantly increased due to skin and proximity eddy-current effects. The skin and proximity losses due to fundamental frequency current have been investigated in literature, but the influence of pulsewidth modulation (PWM) on the skin and proximity losses has not been reported. In this paper, a 2-D finite element method is employed to analyze the skin and proximity losses in a permanent magnet brushless ac machine, in which significant proximity loss exists due to high frequency current ripples induced by the PWM, as confirmed by both theoretical calculation and experiment. The analyses should be generally applicable to other machines.**

***Index Terms*—Brushless ac machine, eddy-current loss, permanent-magnet machine, proximity loss, pulsewidth modulation, skin effect.**

I. Introduction

IT IS well-known that a winding copper loss can be significantly increased due to skin and proximity eddy-current effects [1]–[9]. This is an important consideration in the design of either slotless machines in which the conductors are directly exposed to the time-varying air-gap field [2]–[4] or slotted machines due to the variation of slot leakage field [5]–[7], particularly for machines having high operating frequency, high power density, and high electrical loading.

The proximity eddy-current loss in the conductors may be estimated analytically by neglecting the eddy-current redistribution effect on the field distribution [8]

$$P_e = \frac{\pi d^4 \omega^2 B_n^2}{128 \rho_c} \quad \text{(Watts per unit conductor length)} \qquad (1)$$

where d and ρ_c are the diameter and resistivity of conductor, respectively, and B_n and ω are the peak value and angular velocity of flux density harmonic, respectively.

Paper 2008-EMC-199, presented at the 2008 Industry Applications Society Annual Meeting, Edmonton, AB, Canada, October 5–9, and approved for publication in the IEEE TRANSACTIONS ON INDUSTRY APPLICATIONS by the Electric Machines Committee of the IEEE Industry Applications Society. Manuscript submitted for review November 21, 2008 and released for publication February 2, 2009. First published May 19, 2009; current version published July 17, 2009.

S. Iwasaki, R. P. Deodhar, Y. Liu, and A. Pride are with the U.K. Research Centre, IMRA Europe SAS, Brighton, BN1 9RS, U.K. (e-mail: si@imra-ukrc.com; rd@imra-ukrc.com; yong.liu@edwardsvacuum.com; ap@imra-ukrc.com).

Z. Q. Zhu is with the Department of Electronic and Electrical Engineering, University of Sheffield, Sheffield, S1 3JD, U.K. (e-mail: z.q.zhu@sheffield.ac.uk).

J. J. Bremner is with the Sussex Innovation Centre, Elektro Magnetix Ltd., Brighton, BN1 9SB, U.K. (e-mail: jonathanb@elektro.co.uk).

Color versions of one or more of the figures in this paper are available online at http://ieeexplore.ieee.org.

Digital Object Identifier 10.1109/TIA.2009.2023488

Clearly, the proximity eddy-current loss will increase with the amplitude B_n and angular velocity ω of the flux density harmonic. It can be most effectively limited by reducing the conductor diameter d by using stranded wires or Litz wire for very-high-frequency operation, although this will result in high cost and low packing factor [5], [7].

The proximity eddy-current loss can also be reduced very effectively when the variation of flux density in the region where the conductors are located is reduced. The most significant flux density variation is near the stator slot openings in the slotted machines, and hence, high proximity losses are usually observed in the conductors in this region in both switched reluctance machines [6] and permanent magnet brushless machines [5], [7]. However, the field strength drops very quickly, moving away from the slot opening, and the proximity effect losses can be greatly reduced by leaving some space between the winding and the opening [6], [7] although, in this case, the conductor diameter needs to be reduced and the dc resistance will subsequently be increased; hence, a compromise may be required in order to balance the dc and ac copper losses of the windings.

To date, investigations on the proximity loss in electrical machines are usually based on the finite-element calculation of a 2-D eddy current problem in order to account for the complex slot geometry, as well as the coil location [5]–[7]. However, the proximity loss is usually composed of bundle level and strand level components [9]. Two-dimensional finite-element method cannot model the bundle level loss due to circulating current among strands. It cannot model the twisted strands as well. Although a 3-D finite-element model may be used in these cases, it is usually impractical. Therefore, they are often neglected since the bundled level loss is usually assumed to be minimized by twisting the strands.

In [5]–[7], the proximity loss due to fundamental frequency current has been investigated. However, the influence of pulsewidth modulation (PWM) on the proximity loss has not been reported in literature.

In this paper, a 2-D finite element method is employed to analyze the skin and proximity losses in a flux-switching permanent-magnet (FSPM) brushless ac machine, in which significant proximity loss exists due to high frequency current ripples induced by the PWM, as confirmed by both theoretical calculation and experiment.

This paper is organized as follows. The basic machine topology and operating principle of FSPM machines for traction application will be briefly described first, and its proximity loss issues will be reported. Then, the basics of proximity loss

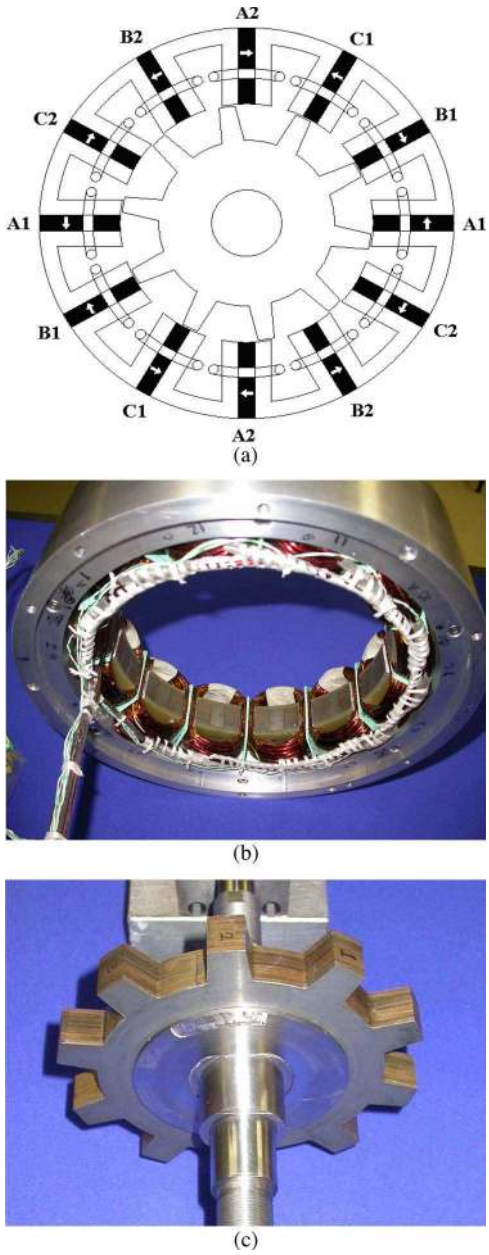

Fig. 1. Three-phase, 12-stator slot, and ten-rotor pole FSPM machine. (a) Schematic. (b) Stator. (c) Rotor.

will be explained, and the influence of iron core, conductor diameter, and number of strands on the proximity loss will be highlighted. Finally, the proximity loss in the prototype machine is analyzed with due account for the conductors in the active lamination stack region and end windings, together with the experimental result. The effect of slot leakage field on ac copper loss will also be shown. The analyses and conclusions should be generally applicable to other machines.

II. FSPM Machine and Proximity Loss

As shown in Fig. 1(a), the stator core of a three-phase FSPM machine [10] comprises of laminated U-shaped segments between which are sandwiched circumferentially magnetized

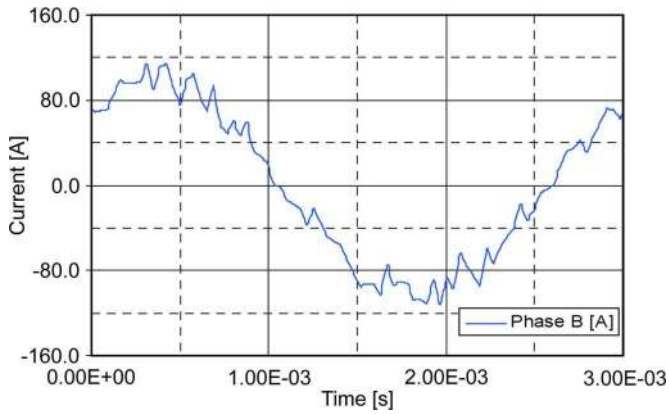

Fig. 2. Phase current waveform at 2 kr/min and 75 Arms.

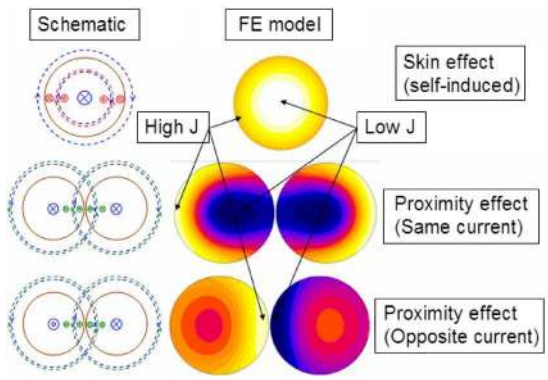

Fig. 3. Illustration of skin and proximity effects; 20 kHz/10 Apk sinusoidal current.

magnets of alternate polarity. The rotor is similar to that of a switched reluctance machine. Although concentrated nonoverlapping winding and salient pole rotor are employed, the back electromotive force waveform is essentially sinusoidal, while the reluctance torque is negligible. The machine is suitable for brushless ac operation. The design specifications of prototype traction motor, Fig. 1, to be investigated are as follows: rated power $= 10$ kW, base speed $= 2500$ r/min, maximum speed $= 10\,000$ r/min, stator outside diameter $= 236$ mm, and axial core length $= 20$ mm. Each phase consists of four coils which are connected in series, with 18 turns per coil. The outside diameter of solid copper is $\varnothing 2.65$ mm. The dc resistances of three-phase windings at 20 °C are measured to be 40.8, 40.54, and 40.54 mΩ, respectively.

The machine is designed to operate at both constant torque and constant power regions. Hysteresis PWM has been employed to produce the sinusoidal phase current. At high speed in the constant power region, the number of PWM switching events is very limited, as it is well known that, even when the inverter operates close to six-step mode, the phase current will be very close to sinusoidal waveform [11]. At relatively low speeds (e.g., below the base speed), the current waveform contains a number of high frequency harmonics due to PWM chopping, Fig. 2. These harmonics introduce eddy currents in conductors, which cause a nonuniform distribution of current density within the cross-sectional area of each conductor.

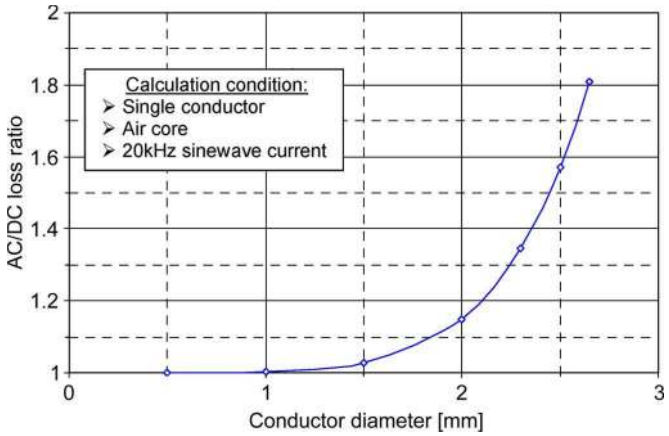

Fig. 4. AC/DC copper loss ratio as a function of conductor diameter.

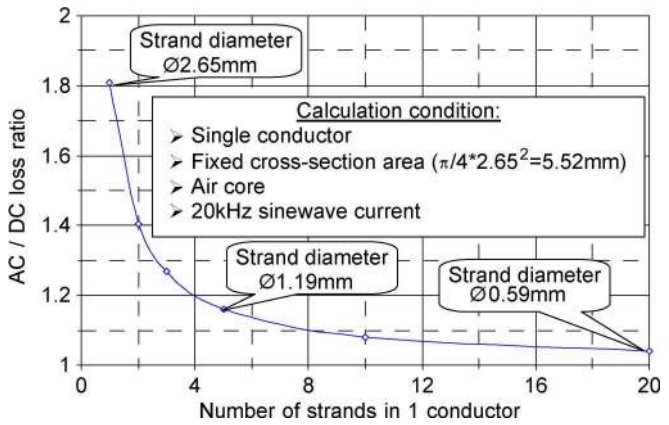

Fig. 5. AC/DC copper loss ratio as a function of number of strands per conductor.

Such nonuniform distribution of current density in a conductor due to its own current is called skin effect, while that due to currents in adjacent conductors is called proximity effect, as shown in Fig. 3.

In order to ease the discussion, the dc and ac copper losses are defined as follows.

1) DC copper loss $= I_{\rm rms}^2 R_{\rm dc}$, where $I_{\rm rms}$ is the rms current and $R_{\rm dc}$ is the dc resistance with due account for temperature rise.
2) AC copper loss = DC copper loss + extra loss due to skin and proximity effects.

A significant loss due to skin and proximity effects is found at operation speed below the base speed. By way of example, for the prototype machine under 2 kr/min/75 Arms hysteresis PWM current control, as will be shown later in this paper, the winding dc copper loss at an operating temperature of 100 °C is 829 W, the finite element calculated and measured extra ac copper losses due to skin and proximity effects are 267.5 and 299 W, respectively, and the finite element calculated extra ac copper loss due to pure sinusoidal current waveform is 132 W only. Although, in the measurement, the loss segregation method is employed and, hence, the measured extra ac copper losses due to skin and proximity effects may exhibit some error, the finite element calculated extra ac copper losses for the actual

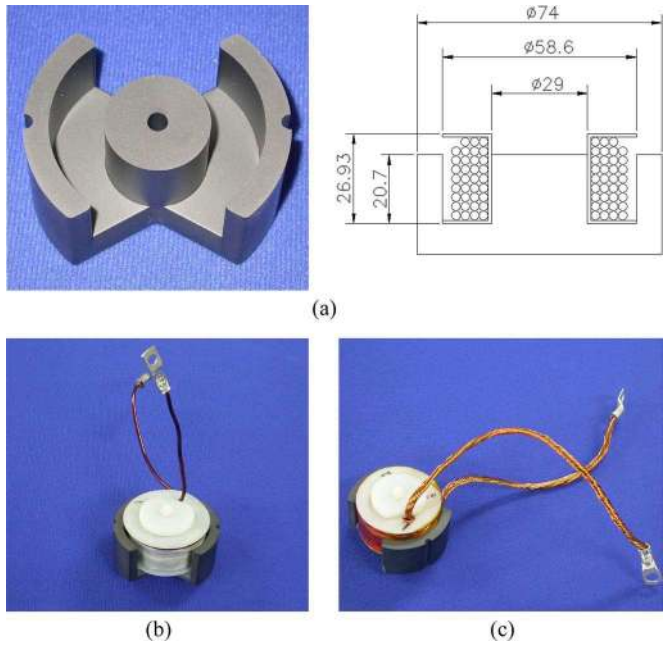

Fig. 6. Samples of pot-core coils. (a) Ferrite pot core. (b) Solid wire; 35 turns × Ø2.65 mm. (c) Stranded wire; 33 turns × 90 strands × Ø0.28 mm.

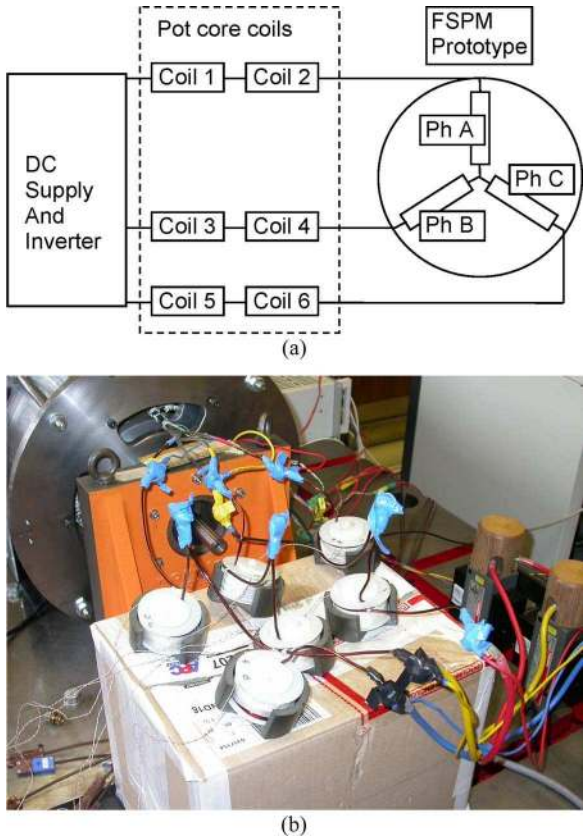

Fig. 7. Pot-core coil connections to motor windings. (a) Schematic. (b) Experimental setup.

current waveform under PWM control and for ideal sinusoidal current waveform having the same rms value are 267.5 and 132 W, respectively. This confirms that the extra ac loss contribution from PWM current harmonics is significant.

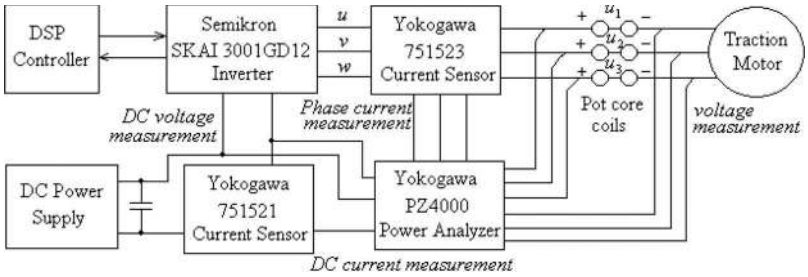

Fig. 8. Schematic of the measurement of ac copper losses in pot-core coils.

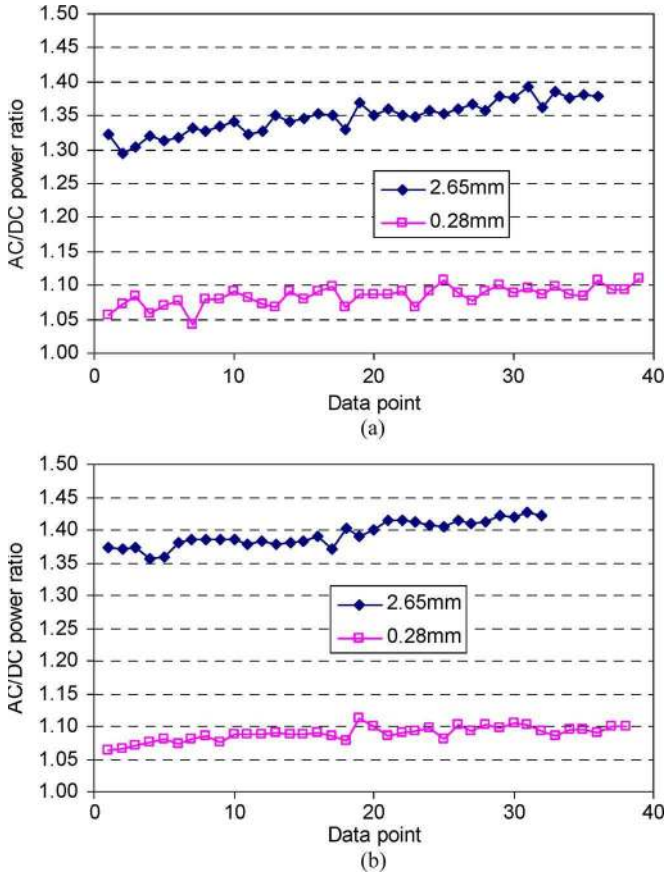

Fig. 9. Measured ac/dc copper loss ratios of pot-core coils with different copper diameters. Hysteresis PWM, 75 Arms. (a) 1000 r/min. (b) 2000 r/min.

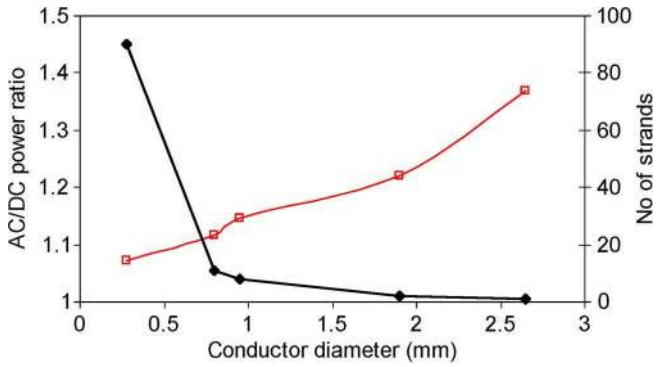

Fig. 10. Variation of the measured ac/dc copper loss ratio with conductor diameter/number of strands of pot-core coils. Hysteresis PWM, 75 Arms, and 2 kr/min.

TABLE I
TWO-DIMENSIONAL FINITE ELEMENT CALCULATED AC COPPER LOSS IN SINGLE SLOT MODEL USING THE MEASURED CURRENT WAVEFORMS, 2 kr/min, 75 Arms, AND HYSTERESIS PWM CHOPPING

Model type	36 conductors (each conductor is Ø2.65mm × L20mm @ 20°C)	18 conductors (each conductor is Ø2.65mm × L20mm @ 20°C)
Core type	Iron core (to simulate active winding length)	Air core (to simulate end-winding length)
Current waveform	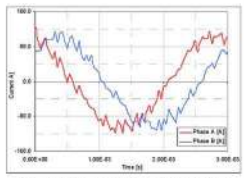 Phase B reversed to take account of 'Go' & 'Return' coil sides in the same slot	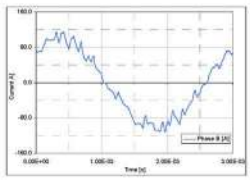
Current density image	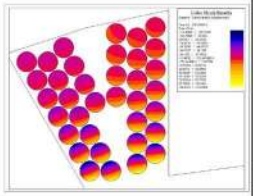	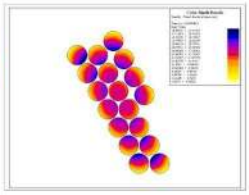
DC copper loss [W]	12.10	5.76
AC copper loss [W]	28.26	6.03
AC/DC copper loss ratio	2.336	1.047

III. AC COPPER LOSS IN CONDUCTORS AND POT-CORE COILS

In order to fully understand the ac copper loss in the prototype traction motor, first, a simple 2-D finite element method is used to calculate the ac/dc copper loss ratio in a single conductor of $diameter = \varnothing 2.65$ mm and $length = 20$ mm, carrying 20 kHz/10 Apk current in airspace, Fig. 3. As expected, Fig. 4 shows that the ac/dc loss ratio is reduced as the conductor diameter is reduced, while Fig. 5 shows that, for the same conductor cross-sectional area, the loss ratio is reduced by increasing the number of strands per conductor.

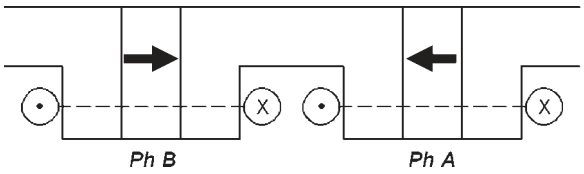

Fig. 11. Phases A and B coil sides in a single slot.

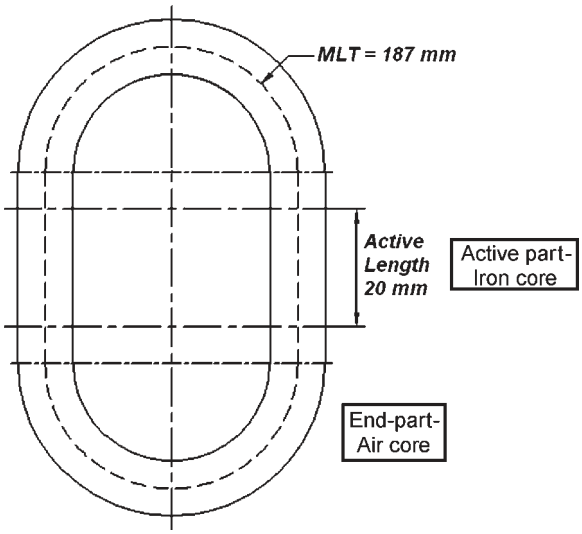

Fig. 12. Coil in traction motor (MLT—mean length of turn, wire diameter = ∅2.65 mm, and no strand).

TABLE II
AC COPPER LOSS IN TRACTION MOTOR WITH ACTUAL CURRENT WAVEFORMS, 2 kr/min, 75 Arms, AND HYSTERESIS PWM CHOPPING

Model type	Combined models in Table I (winding at operating temperature, 100°C)
Core type	Iron core for winding in active length Air core for end winding
Current waveform	Referring to Table I
DC copper loss [W]	829
AC copper loss [W]	1096.5
AC/DC copper loss ratio	1.32
Current density image	Referring to Table I

Second, the ac copper losses in pot-core coils are measured in order to show the increase of proximity effect by the presence of ferromagnetic materials and the reduction of ac winding loss by using multistranded wire and reduced conductor size. A set of six identical pot-core coils using various copper outside diameters, viz., ∅2.65, ∅1.90, ∅0.95, ∅0.8, and ∅0.28 mm (copper: Nexans Magnetemp CA-200), is made. Pot cores are made of commercial ferrites used for high frequency inductors/transformers (RS 212-5094), and all coils have approximately 35 turns (except for ∅0.8- and ∅0.28-mm conductors, where the number of turns is reduced to 33 turns in order to ease winding), but different number of strands, so that the total equivalent cross-sectional area is essentially the same ($\sim$5.5 mm^2). Fig. 6(a) shows the ferrite pot core and its dimensions. Sample pot-core coils are shown in Fig. 6(b) and (c). The details for all pot-core coils and their measured dc resistances and inductances are given in Appendix I.

TABLE III
CALCULATION OF TRACTION MOTOR COPPER LOSS AT 2 kr/min, HYSTERESIS PWM, 75 Arms, AND 100 °C

Active part (length =20+20=40mm) loss	End-winding part (length=147mm) loss	Total (MLT=187mm) loss
DC loss ($3I_{rms}^2R_{dc}$)		
177.3W	651.7W	829.0W
AC copper loss (DC loss + extra AC loss due to skin & proximity effects)		
414.2W (=177.3W×2.336)	682.3W (=651.7W×1.047)	1096.5W
AC/DC copper loss difference: 267.5W (=1096.5W-829.0W)		
AC/DC copper loss ratio: 1.32 (=1096.5W/829W)		

TABLE IV
COMPARISON OF THE CALCULATED AND MEASURED EXTRA AC COPPER LOSSES DUE TO SKIN AND PROXIMITY EFFECTS IN TRACTION MOTOR, 2 kr/min, HYSTERESIS PWM, 75 Arms, AND 100 °C

Calculated (ideal sinusoidal current waveform without PWM)	132W
Calculated	**267.5W**
Measured	**299W**

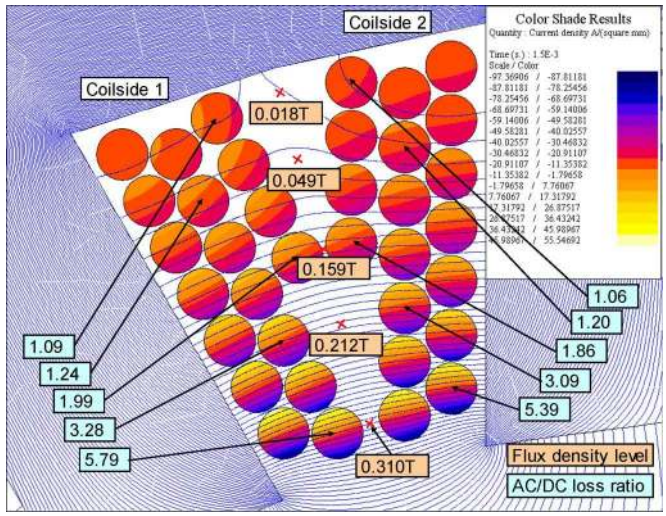

Fig. 13. Relationship between slot leakage field and ac/dc copper loss ratio. Hysteresis PWM, 75 Arms, and 2 kr/min.

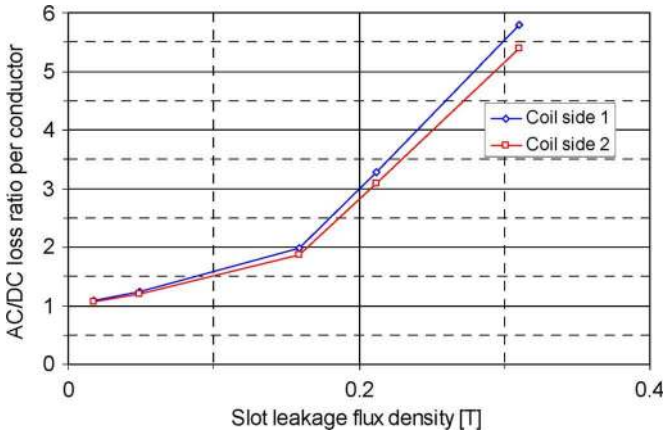

Fig. 14. Effect of leakage flux density on ac/dc copper loss ratio per conductor. Hysteresis PWM, 75 Arms, and 2 kr/min.

TABLE V
DETAILS AND MEASURED DC RESISTANCE AND INDUCTANCE OF POT-CORE COILS

Diameter	Ø2.65 mm		Ø1.9 mm		Ø0.95 mm		Ø0.8 mm		Ø0.28 mm	
Strands	1		2		8		11		90	
Area	5.5 mm^2		5.67 mm^2		5.67 mm^2		5.53 mm^2		5.54 mm^2	
Turns	35		35		35		33		33	
coil	DC Resistance (mΩ)	Inductance μH @ 10kHz	DC Resistance (mΩ)	Inductance μH @ 10kHz	DC Resistance (mΩ)	Inductance μH @ 10kHz	DC Resistance (mΩ)	Inductance μH @ 10kHz	DC Resistance (mΩ)	Inductance μH @ 10kHz
1	14.450	119.02	15.488	137.77	15.990	145.8	16.005	136.8	16.886	136.6
2	14.546	119.82	15.628	135.08	15.895	153.13	15.967	133.2	16.566	136.85
3	14.433	119.07	15.352	137.8	16.000	152.86	15.978	136.3	16.790	135.03
4	14.473	120.77	15.422	137.25	15.970	146.8	16.687	134.4	16.740	136.72
5	14.489	120.21	15.462	136.66	15.920	151.5	16.160	135.5	16.330	135.24
6	14.462	119.92	15.390	137.22	16.107	150.18	16.160	129.9	15.970	132.32

TABLE VI
MEASURED AVERAGE DC AND AC LOSSES OF POT-CORE COILS, 2 kr/min, HYSTERESIS PWM

Wire size, mm	No of strands	Phase A Current, Arms	Phase B Current, Arms	Phase C Current, Arms	DC loss, kW	AC loss, kW	Extra AC loss due to skin & proximity effects, kW	AC/DC loss ratio
2.65	1	73.1	72.5	72.5	0.574	0.785	0.211	1.368
1.9	2	74.4	73.2	72.8	0.634	0.774	0.140	1.221
0.95	8	73.6	72.4	72.3	0.630	0.721	0.091	1.145
0.8	11	73.6	72.6	72.2	0.618	0.690	0.072	1.116
0.28	90	75.1	74.7	74.4	0.628	0.673	0.045	1.072

In order to ensure that similar current waveforms are being used, a pair of pot-core coils are connected in series with each motor phase winding, as shown in Fig. 7, and the voltage terminals of the power analyzer are connected directly across each pair of pot-core coils, as shown in Fig. 8. Pot-core coil temperature is also measured and simultaneously logged with the power analyzer readings.

The dc copper loss is simply calculated from the rms current $I_{\rm rms}$ and dc resistance $R_{\rm dc}$, as well as the coil temperature, as described in Section II, and compared with the ac copper loss measured by the power analyzer, which should include any skin and proximity effects.

Tests were done when the prototype traction motor was fed from a hysteresis PWM inverter, 75 Arms, at 1000 and 2000 r/min, respectively, with the phase current waveforms and their spectra being given in Appendix III. The measured data are listed in Appendix II and summarized in Fig. 9. It can be seen that, at 1000 r/min, the ac/dc copper loss ratio is $\sim$1.35 for $\varnothing$2.65-mm pot-core coils and confirms that the skin and proximity effects are producing a higher resistance than the pure dc resistance. The ac/dc copper loss ratio for $\varnothing$0.28-mm stranded wire pot-core coils is $\sim$1.08, which is significantly lower than the $\varnothing$2.65-mm wire. However, it is found that, for this specific prototype motor, the change in fundamental frequency, i.e., increasing the operating speed from 1000 to 2000 r/min, only slightly increases the ac/dc copper loss ratio, Fig. 9. However, as shown in Fig. 10, the ac/dc copper loss ratio is reduced significantly when the diameter of conductors is reduced and the number of strands is increased, very similar to the case when the conductor is placed in the airspace, Figs. 4 and 5.

IV. INVESTIGATION OF AC COPPER LOSS IN PROTOTYPE TRACTION MOTOR

Table I shows the 2-D finite element calculated loss results based on a single slot model for the prototype traction motor (variation of instantaneous current density distributions in the conductors in the slot being shown in Appendix IV). Each slot contains coil sides from two phases with 18 conductors per coil side (as shown in Fig. 11) and carrying currents captured under test condition (2 kr/min/75 Arms, hysteresis PWM chopping). Each conductor is $\varnothing$2.65 mm $\times$ L20 mm.

It can be seen that the ac copper loss is significantly higher than that of dc copper loss, the ac/dc copper loss ratio being 2.336. For comparison, the ac copper loss in one phase conductors, when they are in airspace, is also calculated, the corresponding ac/dc copper loss ratio being only 1.047. Hence, the ac copper loss is significantly increased due to the presence of iron core. The results obtained from one slot finite element model with/without iron core are subsequently used for calculating the actual ac copper loss due to skin and proximity effects in the prototype traction motor with due account for winding lengths in the active part (iron-cored) and end region (air-cored), Fig. 12. The calculated results are summarized in Table II, while the details of the calculation are given in Table III.

The calculated extra ac copper loss due to skin and proximity effects is compared in Table IV, together with calculated extra ac copper loss due to pure sinusoidal current. Although the ac/dc copper loss ratio of the end winding is lower than that of the active part, the end-winding loss component is dominant in the prototype traction motor, as it has a small aspect ratio of 20 to 236 mm. In addition, the end winding has been approximated

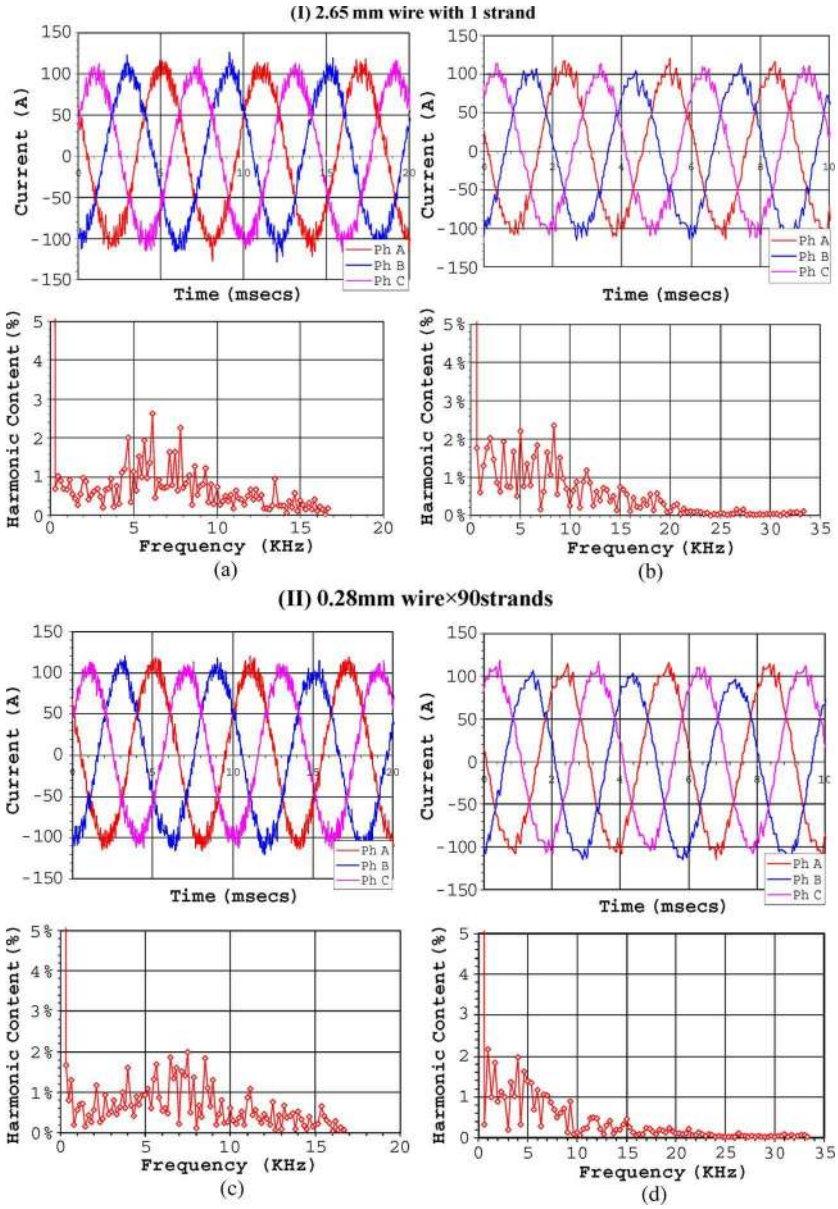

Fig. 15. Phase current waveforms/spectra and ac/dc loss ratio of pot-core coils. (I) 2.65-mm wire with one strand: (a) 1000 r/min (fundamental 167 Hz), $THD = 8.0\%$, and ac/dc copper loss ratio $= 1.35$; (b) 2000 r/min (fundamental 333 Hz), $THD = 7.8\%$, and ac/dc copper loss ratio $= 1.37$. (II) 0.28-mm wire $\times$ 90 strands: (c) 1000 r/min (fundamental 167 Hz), $THD = 7.8\%$, and ac/dc copper loss ratio $= 1.08$; (d) 2000 r/min (fundamental 333 Hz), $THD = 5.9\%$, and ac/dc copper loss ratio $= 1.09$.

as completely air-cored, and the influence of iron core, the curvature of coil shape, etc. on the end-winding ac copper loss calculation has been neglected. Considering the complexities of calculation and also the difficulties in measurement by using the loss segregation method (e.g., the influence of PWM effect on the iron loss was only accounted for by finite element calculation), the agreement can be considered to be good. Most importantly, it confirms the significant influence of PWM on the skin and proximity losses.

It is worth mentioning that the foregoing investigation focuses on the influence of hysteresis PWM chopping on the ac copper loss, and the space vector PWM chopping has also been employed during the investigation of ac copper losses in both pot-core coils and prototype traction motor. Although the loss values are somewhat different, similar trends have been observed, again confirming the influence of PWM on the skin and proximity losses.

V. Effect of Slot Leakage Field on AC Copper Loss

Further investigation of loss distribution within conductors in a single slot shows that there is a correlation between the level of slot leakage field, the location of an individual conductor, and the amount of ac loss in that conductor. This can be clearly seen in Figs. 13 and 14 for the prototype traction motor under the excitation of hysteresis PWM controlled current of 75 Arms. Fig. 13 shows that slot leakage field level is the highest in the slot opening region and the lowest in the slot bottom region. Figs. 13 and 14 also show that the amount of ac copper loss (ac/dc copper loss ratio) is the highest in conductors located

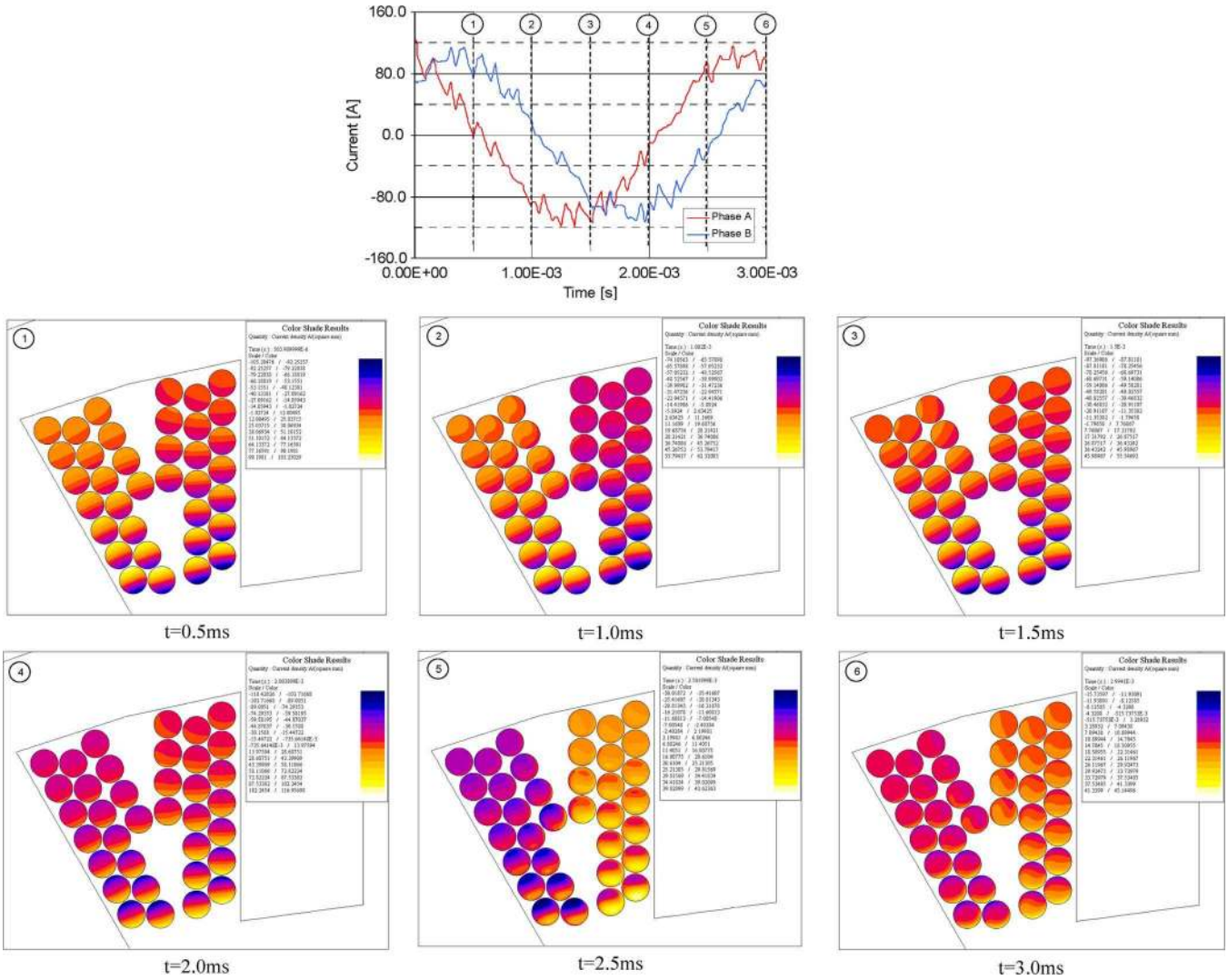

Fig. 16. Variation of finite element calculated instantaneous eddy current density distributions.

in the slot opening region, while it is the lowest in conductors located in the slot bottom region. It shows that the ac copper loss is approximately proportional to the square of slot leakage field. It confirms that, similar to the case of pure sinusoidal current excitation as reported in [7], under PWM controlled current excitation, the relative distribution of ac copper loss in conductors within one slot remains unchanged.

VI. Conclusion

Finite-element method has been employed to analyze the skin and proximity losses in a permanent-magnet brushless ac machine. Skin and proximity losses are significantly increased due to high frequency current ripples induced by PWM, as confirmed by both theoretical calculation and experiment. The analyses and conclusions should be generally applicable to other machines.

Appendix I

See Table V.

Appendix II

See Table VI.

Appendix III
Measured Phase Current Waveforms and Spectra in Pot-Core Coil Test

See Fig. 15.

Appendix IV
Finite Element Calculated Instantaneous Eddy Current Density Distributions

See Fig. 16.

References

[1] E. Levi, *Polyphase Motors—A Direct Approach to Their Design*. New York: Wiley, 1984.

[2] A. A. Arkadan, R. Vyas, J. G. Vaidya, and M. J. Shah, "Effect of toothless stator design on core and stator conductors eddy current losses in permanent magnet generators," *IEEE Trans. Energy Convers.*, vol. 7, no. 1, pp. 231–237, Mar. 1992.

[3] J. Engstrom, F. Magnussen, and H.-P. Nee, "Analytical calculation of winding losses of inverter-fed PM synchronous motors with air-gap windings and surface mounted magnet," in *Proc. EPE*, 1997, pp. 399–404.
[4] R. J. Wang and M. J. Kamper, "Calculation of eddy current loss in axial field permanent magnet machine with coreless stator," *IEEE Trans. Energy Convers.*, vol. 19, no. 3, pp. 532–538, Sep. 2004.
[5] G. J. Atkinson, B. C. Mecrow, A. G. Jack, D. J. Atkinson, P. Sangha, and M. Benarous, "The analysis of losses in high-power fault-tolerant machines for aerospace applications," *IEEE Trans. Ind. Appl.*, vol. 42, no. 5, pp. 1162–1170, Sep./Oct. 2006.
[6] R. B. Inderka, C. E. Carstensen, and R. W. De Doncker, "Eddy currents in medium power switched reluctance machines," in *Proc. IEEE 33rd Annu. PESC*, Jun. 23–27, 2002, pp. 979–984.
[7] P. H. Mellor, R. Wrobel, and N. Mcneill, "Investigation of proximity losses in a high speed brushless permanent magnet motor," in *Conf. Rec. 41st IEEE IAS Annu. Meeting*, Oct. 8–12, 2006, pp. 1514–1518.
[8] P. N. Murgatroyd, "Calculation of proximity losses in multistranded conductor bunches," *Proc. Inst. Elect. Eng. A—Sci. Meas. Technol.*, vol. 136, no. 3, pp. 115–120, May 1989.
[9] C. R. Sullivan, "Optimal choice for number of strands in a Litz-wire transformer winding," *IEEE Trans. Power Electron.*, vol. 14, no. 2, pp. 283–291, Mar. 1999.
[10] Z. Q. Zhu, Y. Pang, D. Howe, S. Iwasaki, R. Deodhar, and A. Pride, "Analysis of electromagnetic performance of flux-switching permanent magnet machines by non-linear adaptive lumped parameter magnetic circuit model," *IEEE Trans. Magn.*, vol. 41, no. 11, pp. 4277–4287, Nov. 2005.
[11] Y. S. Chen, "Motor topologies and control strategies for permanent magnet brushless AC drives," Ph.D. dissertation, Univ. Sheffield, Sheffield, U.K., 1999.

S. Iwasaki was born in Aichi, Japan, in 1948. He received the B.S. degree in electrical engineering from Aichi Institute of Technology, Toyota City, Japan, in 1973.

In 1973, he joined Aisin Seiki Company Ltd., Kariya, Japan, where he was responsible for developing switched reluctance motor systems. In 2002, he joined the U.K. Research Centre, IMRA Europe SAS, Brighton, U.K., as the General Manager, where he is in charge of developing new electric motor and drive technologies.

Rajesh P. Deodhar (M'89–S'94–SM'01) received the B.Eng. degree in electrical and electronics engineering from the University of Mumbai, Mumbai, India, in 1989, the M.Tech. degree in electrical and electronics engineering from the Centre for Electronics Design and Technology, Indian Institute of Science, Bangalore, India, in 1991, and the Ph.D. degree from the University of Glasgow, Glasgow, U.K., in 1996.

He has a global industrial research profile, including work experience at Crompton Greaves in India, Hitachi in Japan, and the Scottish Power Electronics and Electric Drives Laboratory in the U.K. In 1998, he joined the U.K. Research Centre, IMRA Europe SAS, Brighton, U.K., where he is currently a Principal Engineer, working on the design and analysis of a wide range of motors and actuators used in automotive components and systems. He is the coauthor of more than 30 international conference and journal publications and is the holder of more than ten international patents.

Dr. Deodhar has been a recipient of numerous awards, including the Indian Institute of Science Gold Medal in 1991, the IEEE Industry Applications Society (IAS) Annual Meeting Paper Award in 1996, and the IEEE TRANSACTIONS ON INDUSTRY APPLICATIONS Paper Award in 1998. He is a Chartered Engineer and a member of the Institution of Engineering and Technology in the U.K.

Yong Liu received the B.Eng. and M.Sc. degrees in electrical engineering from Zhejiang University, Hangzhou, China, in 1999 and 2002, respectively, and the Ph.D. degree in electrical and electronic engineering from the University of Sheffield, Sheffield, U.K., in 2007.

In 2005, he joined the U.K. Research Centre, IMRA Europe SAS, Brighton, U.K., as a Research Engineer. Since 2008, he has been a Motor and Drive Technologist with Edwards Ltd., West Sussex, U.K. His research interest includes control of electrical machines, particularly permanent-magnet brushless motors and induction motors.

Adam Pride (M'97) received the B.Sc. and M.Sc. degrees in electrical engineering from the University of Manchester Institute of Science and Technology (now the University of Manchester), Manchester, U.K., in 1977 and 1979, respectively.

He was with Froude Consine Ltd., Worcester, U.K., where he worked on research and development of eddy-current dynamometers for automotive engine testing. In 1989, he took part in a four-year around-the-world sailing trip via the Atlantic and Pacific oceans on a 50-foot schooner. Since 1995, he has been with the U.K. Research Centre, IMRA Europe SAS, Brighton, U.K., where he has worked on a wide range of motors and actuators for automotive applications. His particular interests include Halbach magnetized permanent-magnet (PM) machines and analysis of optimum slot/pole combinations for PM machines.

Mr. Pride was awarded with a Silver Medal in the Worshipful Company of Turners/IMechE 1988 Engineering Design Competition for a fast-response motoring/absorbing dynamometer.

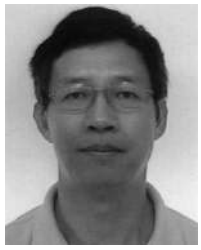

Z. Q. Zhu (M'90–SM'00–F'09) received the B.Eng. and M.Sc. degrees in electrical and electronic engineering from Zhejiang University, Hangzhou, China, in 1982 and 1984, respectively, and the Ph.D. degree in electrical and electronic engineering from the University of Sheffield, Sheffield, U.K., in 1991.

From 1984 to 1988, he was a Lecturer with the Department of Electrical Engineering, Zhejiang University. Since 1988, he has been with the University of Sheffield, where he was initially a Research Associate and was subsequently appointed to an established post as Senior Research Officer/Senior Research Scientist. Since 2000, he has been a Professor of electrical machines and control systems in the Department of Electronic and Electrical Engineering, University of Sheffield, where he is currently the Head of the Electrical Machines and Drives Research Group. His current major research interests include design and control of permanent-magnet machines and drives for applications ranging from electric/hybrid electric vehicles and aerospace to wind power generation, etc.

Jonathan James Bremner was born in the U.K. in 1970. He received the B.Eng. degree (with first class honors) in electronics and electrical engineering and the Ph.D. degree in electrical engineering from the University of Glasgow, Glasgow, U.K., in 1992 and 1996, respectively.

He was a Research Assistant with the Scottish Power Electronics and Electric Drives Laboratory, University of Glasgow, from 1996 to 1998 before taking a position at the Sussex Innovation Centre, Elektro Magnetix Ltd., Brighton, U.K., where he works as a Consultant of electric machines. In over ten years with the company, he has worked on the analysis, design, and implementation of almost all generic types of electric machines for a wide range of industries and applications, including hybrid vehicle propulsion, high-speed generators and spindle motors, automotive actuators, aerospace actuators, and industrial pumps and fans.